

A dampened land use change climate response towards the tropics

M. K. van der Molen^{1,*}, B. J. J. M. van den Hurk¹ and W. Hazeleger¹

¹ *Royal Netherlands Meteorological Institute, P.O. Box 201, 3730 AE De Bilt, the Netherlands*

** now at: Department of Meteorology and Air Quality, Wageningen University and Research Centre (WUR), Postbus 47, 6700 AA Wageningen, The Netherlands, the Netherlands*

Corresponding author : M.K. van der Molen (email: michiel.vandermolen@wur.nl, telephone: +31-317-482104, fax:+31-317-482811)

Abstract

In climate simulations we find a pronounced zonal gradient of climate response to land cover change. Climate response approaches zero in the tropics, and increases towards the poles. The zonal gradient in climate response to land cover change results from damping feedbacks in the tropics, rather than from polar amplification. The main cause for the damping in the tropics is the decrease in cloud cover after deforestation, resulting in increased incoming radiation at the surface and a lower planetary albedo, both counteracting the increase in surface albedo with deforestation. In our simulations, deforestation was also associated with a decrease in sensible heat flux but not a clear signal in evaporation. Zonal differences in climate response have implications for attribution of observed climate change, as well as for climate change mitigation strategies.

Keywords

land use change; deforestation; climate response; regional climate; global climate model

1 Introduction

The currently observed change in global mean temperature can be attributed to changes in the radiation balance of the earth as a result of anthropogenic changes in (a.o.) greenhouse gas concentration, aerosols and land cover (the so-called radiative forcing) and feedbacks of the climate system. The most important radiative forcing of land cover change is the change in albedo and the subsequent change in net radiation in relation to deforestation and/or afforestation. Land cover change has a distinct spatial distribution because of the regional differences in the need for agricultural lands in association with cultural history and the natural distribution of biomes over climate zones. Here we focus on the regional distribution of the feedbacks, of which the most important ones are the changes in evaporation and clouds.

Land cover has changed due to anthropogenic activity: from 1870 to 1992 the fraction of forests on land has decreased from 0.43 to 0.36 (Klein Goldewijk 2001, Ramankutty and Foley 1999, Section 2b), and still the deforestation continues at unprecedented rates. The corresponding increase in albedo has a negative radiative forcing (Forster et al. 2007) with a magnitude of roughly 20% of the radiative forcing of increased CO₂ concentrations in the same period. For these reasons, land cover change is a matter of substantial interest in climate change studies.

The albedo change of land cover change and the associated change in temperature may provoke feedbacks leading to amplification or damping of the initial forcing of the climate system. Examples of mechanisms where feedbacks are involved are 1) the intimate link between land cover change, albedo and energy partitioning at the surface, implying a great potential to actively change boundary layer processes; 2) the impact of clouds on the radiation budget, which is large relative to the radiative forcings of land cover change and CO₂. Changes in cloud formation may form an important feedback to land cover change, because the formation of clouds is connected to the surface fluxes of water vapor and sensible heat: the first is one of the sources of moisture and the second generates the vertical mixing affecting cloud formation. Such feedbacks and their spatial distribution determine the response of climate to the initial albedo change. The interactions between forcing and feedback make the use of complex earth

system/climate models inevitable to quantify the climate response to land cover change.

A number of studies have used global circulation models (GCM's) to study land cover change, some focusing on the tropics (Polcher and Laval 1994, McGuffie et al. 1995, Zhang et al. 1996a,b) and some on the global changes (Zhao et al. 2001, Bounoua et al. 2002, Matthews et al. 2004, Feddema et al. 2005). Pitman et al. (2009) present a concise model intercomparison of the effects of land cover change in the context of the 'Land Use Change – IDentification of robust impacts' (LUCID) project. Results analyzed in this paper are contributed to LUCID. We focus on the regional differences of climate response to land cover change, which have received little attention to date. Regional differences in climate response may have implications for future climate change projections, as well as for designing climate change mitigation strategies. In this perspective, it is the objective of this study to explore how the climate response to land cover change differs regionally in a climate model, and to explain this regional variation. We employ the General Circulation Model (GCM) called EC-Earth to estimate the climate response to land cover change on surface temperature, short- and longwave radiation, cloud cover, and sensible and latent heat fluxes.

2 Methods

To perform the simulations, the EC-Earth global circulation model is used (Haarsma et al. 2009, Hazeleger et al 2010; see eearth.knmi.nl). The model is a derivative of the Operational Seasonal Forecast System 3 of the Integrated Forecast System (IFS) of the European Centre for Medium-Range Weather Forecasts (ECMWF). The atmospheric model version is very similar to IFS cycle 31r1, with spectral truncation T95 and 40 vertical levels. The ocean was represented by prescribed sea surface temperatures (SST) and sea-ice concentration (SIC), varying monthly and inter-annually after the Hadley Centre Ice and Sea Surface Temperature data set (Rayner et al. 2000, 2003). The global mean SST increased 0.33 °C between the pre-industrial and present-day era, whereas the global mean SIC decreased -0.6 % (from 6.2% to 5.6%) (Fig. 1). Four experiments were performed, 1) a 'reference' (r) experiment, with pre-industrial (1870) land cover and CO₂ concentration; 2) a 'modified vegetation' (v) experiment, where land cover was changed to the 1992 distribution (Fig. 2); 3) a

‘modified CO₂ concentration’ (c) experiment, where CO₂ concentration was changed to the 1992 level; and 4) a ‘modified vegetation and CO₂ concentration’ (vc) experiment, where both land cover and CO₂ concentration were changed to the present-day (1992) distribution/level. SST and SIC follow the CO₂ concentration.

Each experiment consisted of 5 ensemble runs of 10-year duration. In each consecutive run, the year of the SST and SIC was advanced 5 years, starting in 1870 for the ‘r’ and ‘v’ runs and in 1972 for the ‘c’ and ‘vc’ runs. Hence each experiment covers in total 30 years with overlapping ensemble members. The atmosphere was always initialized as on 1 January 1990. Potential spin-up errors were checked for by comparing soil moisture for the first year of a simulation with the corresponding overlapping simulation, but the variability between years was generally larger than the difference between overlapping years. Therefore we use the complete time series in the analyses. The concentrations of CH₄, N₂O, CFC11 and CFC12 were changed in concert with the CO₂ concentration changes. Time series of the fractional cover of pasture and crops were obtained from Klein Goldewijk (2001) and Ramankutty and Foley (1999), respectively (Fig. 2), and implemented in the land surface scheme of EC-Earth. 20 different plant functional types are discerned, that are distributed into high and low vegetation types (Van den Hurk et al, 2000). Each grid cell is attributed only one dominant high vegetation type and one low vegetation type, with assigned fractions for each. The vegetation type determines vegetation characteristics such as leaf area index, surface roughness, minimum stomatal resistance and root depth. Originally, EC-Earth uses a satellite derived monthly background albedo map, but for the purpose of this study, we used albedo maps derived by correlation of this background albedo with fraction of each vegetation type, on a monthly and zonal mean basis. Monthly albedo fields were thus produced that correspond with the vegetation maps for 1870 and 1992. Table 1 indicates the typical EC-Earth albedo of ‘high’ and ‘low’ surface types and their relative distribution over the Earth in 1870 and 1992 according to Ramankutty and Foley (1999) and Klein Goldewijk (2001). Using this approach, land cover change caused a 1.4% increase in surface albedo over this period. The model output data are presented as temporal means on a 1° by 1° grid.

The Figs. 3-7 show the change of a number variables with the change in albedo in bins. The significance of the slope of the linear regression line through the raw data points has been tested using Student's t-test, and α , the probability of exceedence, and r^2 are shown in the figures, both for the NH mid latitudes and the tropics.

3 Results

3.1 Temperature response

Land cover change and the associated albedo change cause a change in the radiation balance of the Earth, with a consequent change in temperature. Fig. 3 shows that the temperature changes increase with the albedo changes. The temperature changes with albedo are larger in the Northern Hemispheric (NH) mid-latitudes (45-60°N) than in the tropics (30°S - 30°N). The grid cell average albedo changes in other climate zones are very small, which is why these zones are omitted in Fig. 3. The temperature responses are very similar in the simulations at historic (v-r) and present-day CO₂ concentration and SST/SIC (vc-c). This is a strong indication that different feedback mechanisms are acting in the mid-latitudes than in the tropics.

3.2 Shortwave radiation response

The change in net shortwave radiation at the surface with a unit change of albedo depends on the global radiation, and is therefore strongly correlated with latitude. Fig. 4 shows that the expected change in surface net radiation due to the albedo change (thin lines) is larger in the tropics than in the mid-latitudes due to the larger amounts of global radiation. In contrast to the expected change in net radiation, the actual change in net radiation is smaller in the tropics than in the mid-latitudes. Apparently there is a strong damping feedback mechanism acting in the tropics. In the mid-latitudes, the change in net radiation resembles the radiative forcing, suggesting the absence of (net) feedbacks.

3.3 Cloud feedback

The damping feedback in the tropics is partly explained by a regional decrease in total cloud cover (Fig. 5a): at the top of the atmosphere (TOA) a reduced cloud

cover results in a lower Earth albedo, counteracting the increasing albedo at the surface. At the surface a reduced cloud cover increases the incoming and net shortwave radiation, thus counteracting the effect of the albedo increase. Fig. 5a shows that the cloud cover indeed decreased in the tropics by about 1% in the ‘v-r’ and ‘vc-c’ simulations, whereas it increased slightly in the NH mid-latitudes. In the tropics, the decrease in total cloud fraction is primarily caused by the reduction in high clouds (higher than 6-7 km, Fig. 5b), whereas the fraction of low clouds (lower than about 2 km, Fig. 5c) does not change much. In the mid-latitudes, the slight increase in total cloud fraction is the net effect of a shift from high clouds to low clouds (Fig. 5b and c). Ignoring possible effects of cloud overlap assumptions, this explains the relatively small compensation of surface shortwave radiation in response to surface albedo changes.

3.4 Bowen ratio

Fig. 6 shows that the sensible heat flux (H) is reduced both in the tropics and in the mid-latitudes by a maximum of about 10 W m^{-2} , which is in the same order as the reduction in net shortwave radiation. There is a slight decrease in latent heat flux (LE) in the tropics ($1-3 \text{ W m}^{-2}$) at historic CO_2 concentrations. As a consequence, the boundary layer becomes cooler, somewhat dryer (in the tropics) and probably also shallower. These have counteracting effects on the lifting condensation level and the cloud fraction, consistent with the small change in low cloud cover in the tropics. However, the changes in evaporation are smaller at present day CO_2 -concentrations, implying that this feedback is not very robust. Apparently there is not a strong relation between the change in albedo and the change in latent heat flux, which would make it hard to explain why the cloud fraction changes in the tropics, and not in the NH mid-latitudes. However, Fig. 7 shows that the latent heat flux is stronger correlated to low cloud cover in the tropics than in the NH mid-latitudes. This implies that a drop in albedo causes quite variable responses on LE (fig 6b), but the resulting change in LE nevertheless explains to a certain degree the change in low cloud fraction, in the tropics. The variable response of LE to albedo may be expected, because LE does not only depend on albedo, but also in available energy, vapour pressure deficit and soil moisture. It may also be expected that the response of low clouds to LE is stronger in the tropics than in the mid-latitudes, because in the tropics clouds are

more often caused by local convection and in the mid-latitudes clouds are more often caused by synoptic weather systems.

As a result of the changed surface temperatures and cloud fractions, the net longwave radiation also changes, with distinct differences between the NH mid-latitudes and the tropics (Fig. 8). The changes in longwave radiation are as expected from the change in cloud cover, and oppose the effect of cloud cover on shortwave radiation.

3.5 Zonal climate response

As a result of the different feedbacks, the climate response ΔT is not homogeneously distributed over the globe (Fig. 9a). Here the climate response is scaled with Δalbedo , to account for the varying degree of land cover change. A strong latitudinal gradient is observed, where climate response $\Delta T / \Delta \text{albedo}$ is nearly zero in the tropics and increasing to a (negative) maximum in the mid-latitudes. This is also clearly visible in the zonal average climate response (Fig. 8b).

The values presented in Fig. 9a represent the average local climate response over the land area where the albedo change is larger than ± 0.002 (this lower limit in albedo change is required to obtain a stable ratio). The local approach gives an underestimation of the climate response, because advection and feedback propagation may cause non-local temperature changes. Fig. 8b also shows the non-local zonal climate response computed as the ratio of the zonal average temperature change and the zonal average albedo change, thus including non-local temperature changes. This non-local climate response is indeed somewhat larger (more negative, Fig. 9b).

4 Discussion

It is known that the climate response to a given radiative forcing may depend on the characteristics in terms of nature, latitude, and altitude of the forcing (*cf.* Hansen et al. 1997, Harvey 2000, Boer and Yu 2003a,b). However, to our knowledge the distinct zonal gradient in climate response to land cover change has not been reported earlier. The zonal gradient in climate response to land cover change has implications for explaining observed temperature changes in regions affected by land cover change. It also impacts the efficiency of afforestation

programs aimed at mitigating climate warming by sequestering carbon dioxide from the atmosphere. Our model results suggest that afforestation is accompanied in the NH mid-latitudes with climate warming, whereas it is nearly temperature neutral in the tropics (apart from the effect of the mitigated greenhouse gas effect). Bonan (2008) also discusses the zonal differences of climate impact of forests, and argues that the most important biophysical impacts of tropical and boreal forests are evaporative cooling and warming by snow masking, respectively. The negative radiative forcing of deforestation would thus be accompanied by warming feedbacks in the tropics and cooling feedbacks in the northern latitudes. This is consistent with our results, although we do not find substantial changes in LE in the tropics, or amplified changes in albedo in the boreal zone.

The term ‘polar amplification’ is often used in global warming studies to emphasize that global warming due to the enhanced greenhouse gas effect is amplified towards the poles as a result of the snow-albedo feedback. In the case presented here it is more appropriate to use the term ‘tropical damping’, because there is no evidence of the presence of amplifying feedbacks in the NH mid-latitudinal shortwave radiation, whereas there is evidence of damping feedbacks in the tropics (Figs. 4 and 5).

The evidence of the damping feedback in the tropics is most convincingly seen in Fig. 4, showing that the actual decrease in net shortwave radiation with albedo increase is much smaller than expected. This can only be explained by an increase in incoming shortwave radiation, which must be related to a reduction in cloud fraction. The large standard deviations in the ΔLE (Fig. 6b) show that there is quite some variation, suggesting that the general trend of decreased cloud cover reflects the net balance of the varying influences of Bowen ratio, convection strength and boundary layer height. However, there is a stronger relation between the change in LE and the low cloud fraction (Fig. 7).

Two potential explanations for the difference between ‘polar amplification due to the enhanced greenhouse gas effect’ and ‘tropical damping due to land cover change’ are 1) that the majority of land cover change does not extend far enough to the North for the snow-albedo feedback to have a pronounced effect in areas affected by land cover change, and 2) that the climate response to land cover change has a pronounced diurnal cycle, in concert with global radiation, and

therefore has a great potential to affect convective cloud development (Fig. 5).

The greenhouse gas effect in contrast has no pronounced diurnal cycle. The latitudinal gradient of global radiation does not explain the observed zonal gradient in climate response, because the larger amount of global radiation towards the tropics would be expected to increase the radiative forcing and climate response, which is opposite to our model results.

The specific LUCID experimental setup (Pitman et al., 2009) with fixed SST and SIC suppresses temperature changes over the ocean in response to vegetation change. The fixed SST and SIC in practice turn the oceans into potentially unlimited sources or sinks of heat and moisture. This is illustrated by the changes in net oceanic surface sensible and latent heat fluxes in response to land cover change: $\Delta H = +0.017 \text{ W m}^{-2}$ and $\Delta LE = +0.033 \text{ W m}^{-2}$. The oceanic heat release is a response to the cooling of the atmosphere, demonstrating that LCC induced cooling has non-local effects on the energy balance, although the ocean temperature does not respond in this experimental setup. However, further studies with coupled ocean models are foreseen. Pitman et al. (2009) show that in the LUCID model intercomparison, EC-Earth is among the three models with the strongest temperature changes. Like EC-Earth, every participating model has the most pronounced temperature changes in the NH mid-latitudes.

Pitman et al. (2009) emphasize that the choices in the surface / vegetation model formulation with respect to short-term variation in surface conductance of water vapor and heat, and particularly to seasonal variation in surface roughness, leaf area index and phenology, as well as the parameterization of different (agricultural) vegetation types has important implications for the model's climate sensitivity to land cover change. In this respect, EC-Earth, with seasonally fixed roughness and leaf area index and uniform soil types across the globe (van den Hurk et al., 2000) currently takes a middle position considering complexity among the 4 models without dynamic vegetation participating in LUCID.

However, the response of latent heat flux (LE) to land cover change appears quite contrasting between the models: some models simulate decreasing LE after deforestation in all climate zones (IPSL, CCAM, SPEEDY), one model simulates increasing LE (CCSM) and other models simulate mixed and/or zonally varying responses (ARPEGE, ECHAM5, EC-Earth). Pitman et al. (2009) argue that there

is no agreed upon best practice or large-scale calibration protocol, and as a result the climate response to land cover change depends on the model formulation. In South America a contrasting climate response pattern appears as a function of continentality, with cooling near the coast and warming further inland (Fig 8a). This shows that different feedback mechanisms are active. In continental conditions these are often related to cloud cover (convective or stratiform) and water vapor recycling, and in maritime conditions often related to sea breezes (van der Molen et al., 2006).

5 Conclusions

Simulations with the EC-Earth climate model indicate a strong zonal gradient in climate response to land cover change: the climate response is nearly zero in the tropics and increases towards the NH mid-latitudes. Classical theory is that climate warming amplifies towards the poles, because of the snow-albedo feedback. However, in our simulations, the change in net radiation resembles the radiative forcing in the NH mid-latitudes, whereas it is much smaller in the tropics. This indicates that (net) damping feedbacks are present in the tropics, but not in the NH mid-latitudes. We show that in our model a decrease in cloud cover after deforestation is responsible for this ‘tropical damping’.

Distinguishing zonal differences in climate response to land cover change is important for attribution of climate change, and may have implications for the effectiveness of afforestation programs to mitigate climate change due to increasing CO₂ concentrations. Simulations of the impact of land cover change on climate by different climate models often provide contrasting results, as a consequence of defensible differences in model formulations. The climate response is a useful parameter for climate model intercomparisons, and we aim to contribute to such intercomparisons with this publication.

Acknowledgements

We thank Xueli Wang for her help setting up the experiments. The organizers of the LUCID campaign are acknowledged, in particular Nathalie de Noblet, Andy Pitman and Faye Cruz. The Dutch Research Organization (NWO) sponsored parts of this study.

References

- Boer, G.J. and B. Yu (2003a) Climate sensitivity and response. *Clim Dyn* 20: 415–429, doi:10.1007/s00382-002-0283-3
- Boer, G.J. and B. Yu (2003b) Climate sensitivity and climate state *Clim Dyn*, 21:167-176. doi:10.1007/s00382-003-0323-7
- Bonan, G.B. (2008) Forests and climate change: forcings, feedbacks and climate benefits of forests. *Science* 320:1444-1449
- Bounoua, L., R. Defries, G.J. Collatz, P. Sellers and H. Kahn (2002) Effects of land cover conversion on surface climate. *Clim. Chang* 52: 29-64
- Feddema, J.J., K.W. Oleson, G.B. Bonan, L.O. Mearns, L.E. Buja, G.A. Meehl, W.M. Washington (2005) The importance of land-cover change in simulating future climates. *Science* 310:1674-1678
- Forster, P., V. Ramaswamy, P. Artaxo, T. Berntsen, R. Betts, D.W. Fahey, J. Haywood, J. Lean, D.C. Lowe, G. Myhre, J. Nganga, R. Prinn, G. Raga, M. Schulz and R. van Dorland (2007): Changes in Atmospheric constituents and in radiative forcing. In: S. Solomon, D. Qin, M. Manning, Z. Chen, M. Marquis, K.B. Averyt, M. Tignor and H.L. Miller (Eds) *Climate change 2007: The physical basis, contribution of Working group I to the fourth assessment report of the Intergovernmental Panel of Climate Change*, Cambridge University Press, Cambridge, United Kingdom and New York, NY, USA, 129-234
- Haarsma, R.J., F.M. Selten, B.J.J.M. van den Hurk, W. Hazeleger en X. Wang (2009) Drier Mediterranean Soils due to Greenhouse Warming bring easterly Winds over Summertime Central Europe. *Geophys. Res. Lett.* 36:L04705. doi:10.1029/2008GL036617
- Hansen, J., M. Sato and R. Ruedy (1997) Radiative forcing and climate response. *J. Geophys. Res.* 102 (D6):6831-6864
- Harvey, L.D.D. (2000) *Global Warming, the hard science*. Prentice-Hall, Harlow, UK
- Klein Goldewijk, K. (2001) Estimating global land-use change within the past 300 years: the HYDE database. *Glob. Biogeochem. Cycl.* 15:417-433
- Hazeleger, W., Severijns, C., Semmler, T., Stefanescu, S., Yang, S., Wang, X., Wyser, K., Baldasano, J. M., Bintanja, R., Bougeault, P., Caballero, R., Dutra, E., Ekman, A. M. L., Christensen, J. H., van den Hurk, B., Jimenez, P., Jones, C., Kallberg, P., Koenigk, T., McGrath, R., Miranda, P., van Noije, T., Parodi, J. A., Schmith, T., Selten, F., Storelvmo, T., Sterl, A., Tapamo, H., Vancoppenolle, M., Viterbo, P., and Willen, U. (2010) EC-EARTH: A seamless earth system prediction approach in action. *Bull. Am. Meteorol. Soc.*, accepted for publication
- Matthews, H.D., A.J. Weaver, K.J. Meissner, N.P. Gillett and M. Eby (2004) Natural and anthropogenic climate change: incorporating historical land cover change, vegetation dynamics and the global carbon cycle. *Clim. Dyn.* 22:461-479
- McGuffie, K., A. Henderson-Sellers, H. Zhang, T.B. Durbidge, A.J. Pitman (1995) Global climate sensitivity to tropical deforestation. *Glob. Plan. Chang.* 10:97-128
- Pitman, A.J., N. de Noblet-Ducoudré, F.T. Cruz, E.L. Davin, G.B. Bonan, V. Brovkin, M. Claussen, C. Delire, L. Ganzeveld, V. Gayler, B.J.J.M. van den Hurk, P.J. Lawrence, M.K. van der

- Molen, C. Müller, C.H. Reick, S.I. Seneviratne, B.J. Strengers and A. Voldoire (2009) Land-Use and climate via the LUCID intercomparison study: implications for experimental design in AR5. *Geophys. Res. Lett.* 36:L14814. doi:10.1029/2009GL039076
- Polcher, J. and K. Laval (1994) The impact of African and Amazonian deforestation on tropical climate. *J. Hydrol.* 155:389-405
- Ramankutty, N. and J.A. Foley (1999) Estimating historical changes in global land-cover: croplands from 1700 to 1992. *Glob. Biogeochem. Cycl.* 13:97-1027
- Rayner, N.A., D.E. Parker, E.B. Horton, C.K. Folland, L.V. Alexander and P. Frich (2000) The HadISST1 Global Sea-Ice and Sea Surface Temperature Dataset, 1871–1999. Hadley Center Technical Note 17. Exeter, UK
- Rayner, N.A., D.E. Parker, E.B. Horton, C.K. Folland, L.V. Alexander, D. Rowell, E.C. Kent and A. Kaplan (2003) Global analyses of sea surface temperature, sea ice, and night marine air temperature since the late nineteenth century. *J. Geophys. Res.* 108:4407. doi: 10.1029/2002JD002670
- Van den Hurk, B.J.J.M., P. Viterbo, A.C.M. Beljaars and A.K. Betts, 2000: Offline validation of the ERA40 surface scheme. ECMWF TechMemo 295; see <http://www.ecmwf.int/publications/library/ecpublications/pdf/tm/001-300/tm295.pdf>. Reading, UK
- Van der Molen, M.K., A.J. Dolman, M.J. Waterloo and L.A. Bruijnzeel (2006) Climate is affected more by maritime than by continental land use change: a multiple scale analysis. *Glob. Plan. Chang.*, 54 (1-2):128-149, doi:10.1016/j.gloplacha.2006.05.005
- Zhang, H., A. Henderson-Sellers and K. McGuffie (1996a) Impacts of tropical deforestation. Part I: Process analysis of local climatic change. *J. Clim.* 9:1497-1517
- Zhang, H., K. McGuffie and A. Henderson-Sellers (1996b) Impacts of tropical deforestation. Part II: The role of large-scale dynamics. *J. Clim.* 9:2498-2521
- Zhao, M., A.J. Pitman and T. Chase (2001) The impact of land cover change on the atmospheric circulation. *Clim. Dyn.* 17:467-477

Table 1 Land cover distribution and albedo in 1870 (the ‘pre-industrial’ year in our simulations) and 1992 (the ‘present-day’ year in our simulations), and the corresponding weighted surface albedo

Surface type	Albedo	Surface fraction A.D.	
		1870	1992
Ocean	0.07	0.72	0.72
Low vegetation	0.20	0.10	0.12
High vegetation	0.13	0.12	0.10
Bare ground	0.25	0.03	0.03
Ice	0.50	0.03	0.03
Surface albedo		0.1087	0.1102

Figure Captions

Fig 1 Change in **a** SST and **b** SIC between the present-day and pre-industrial experiments

Fig 2 Change in **a** the fraction of high vegetation (present-day – pre-industrial) and **b** the resulting change in surface albedo

Fig 3 The change in surface temperature as a function of change in albedo computed from the difference between the EC-Earth simulations at historic CO₂ concentration (v-r, solid lines) and at present-day CO₂ concentration (vc-c, dotted lines). The α values represent the probability of exceedence, indicating that the temperature trends for the NH mid latitudes and tropics are both tested significantly different from 0 with the Student t-test

Fig 4 The change in net shortwave radiation as a function of change in albedo computed from the difference between the EC-Earth simulations at historic (v-r, solid lines) and at present-day CO₂ concentration, SST and SIC (vc-c, dotted lines). The thin lines without markers represent the direct shortwave radiative effect of albedo change: incoming SW radiation \times (1 - Δ albedo), thus including the effect of clouds in the reference simulation (solid: NH mid-latitudes, dashed: tropics). The deviation from the straight line (red arrow) indicates the impact of feedbacks. The figure applies to the surface, but is very similar for the TOA. The actual changes in net radiation are significantly different from the expected ones, with exceedence probabilities α

Fig 5 The change in **a** total, **b** high and **c** low cloud cover fraction as a function of change in albedo computed from the difference between the EC-Earth simulations at historic CO₂ concentration (v-r, solid lines) and at present-day CO₂ concentration (vc-c, dotted lines). α indicates the exceedence probability of the slopes relative to a flat line

Fig 6 The change in surface sensible **a** and latent **b** heat flux as a function of the change in computed as the difference between the EC-Earth simulations at historic CO₂ concentration (v-r, solid lines) and at present-day CO₂ concentration (vc-c, dotted lines). α indicates the exceedence probability of the slope of the linear regression line on the raw data

Fig 7 The change in low cloud fraction as a function of the change in latent heat flux between the EC-Earth simulations at historic CO₂ concentration (v-r, solid lines) and at present-day CO₂ concentration (vc-c, dotted lines). α indicates the exceedence probability of the slope of the linear regression line on the raw data

Fig 8 The change in net longwave radiation as a function of the change in albedo computed as the difference between the EC-Earth simulations at historic CO₂ concentration (v-r, solid lines) and at present-day CO₂ concentration (vc-c, dotted lines). α indicates the exceedence probability of the slope of the linear regression line on the raw data

Fig 9a spatial distribution of climate response to land cover change, scaled with the albedo change. Albedo change and temperature response are computed on a monthly basis and displayed as annual mean. Areas where the albedo change is less than 0.002 are masked out **b** zonal average

climate response: the blue line represents the zonal average of the numbers displayed in (a), and the red line represents the zonal average $\Delta T / \Delta$ albedo over land, thus including non-local temperature changes, over latitudinal bands of 20° to reduce cross-zonal temperature advection

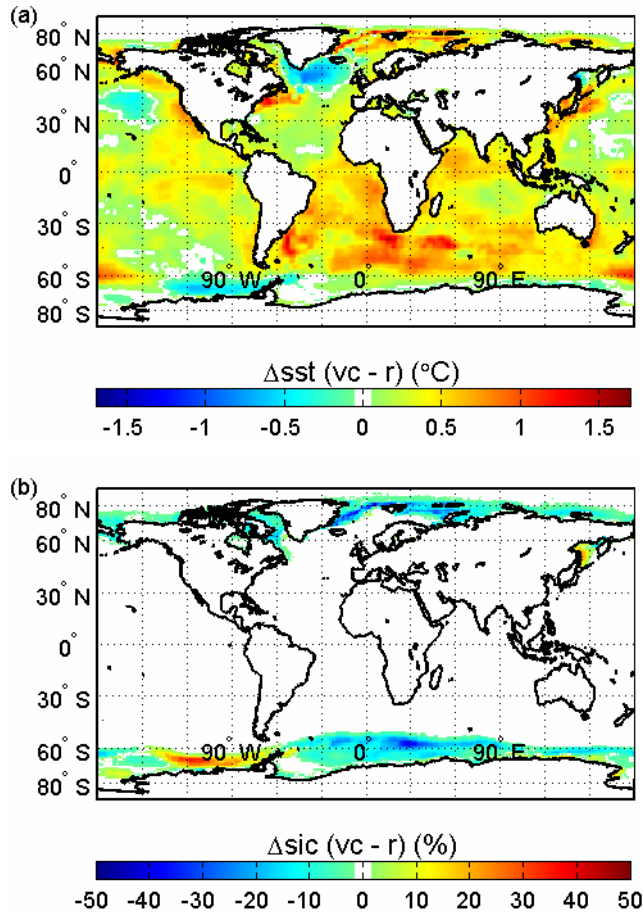


Fig 1 Change in **a** SST and **b** SIC between the present-day and pre-industrial experiments

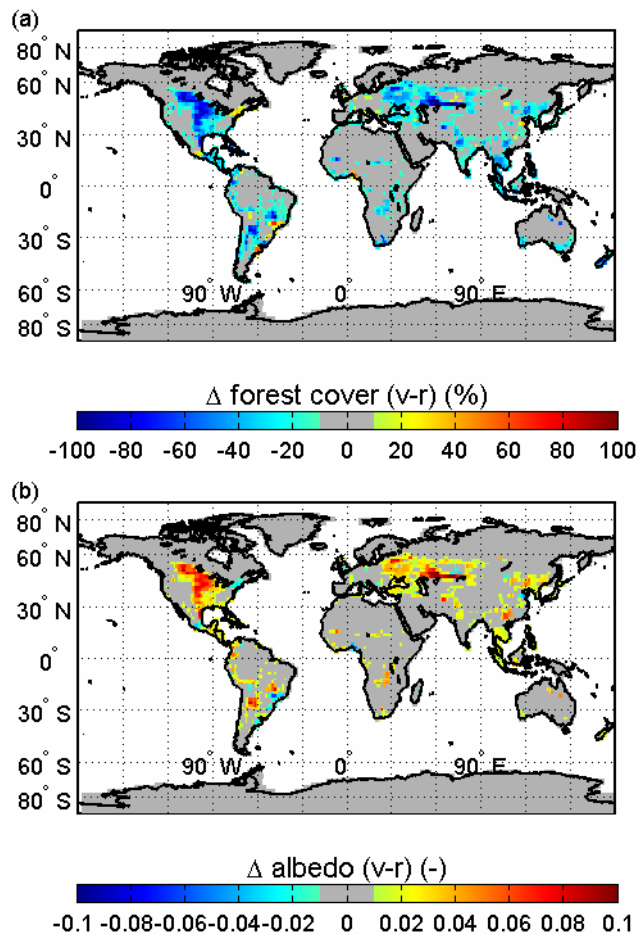


Fig 2 Change in **a** the fraction of high vegetation (present-day – pre-industrial) and **b** the resulting change in surface albedo

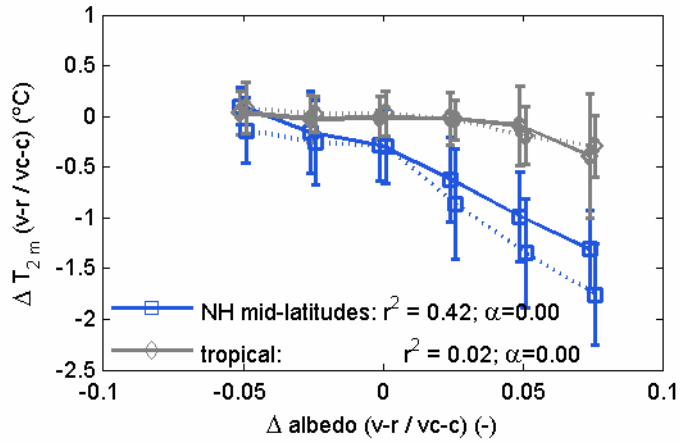


Fig 3 The change in surface temperature as a function of change in albedo computed from the difference between the EC-Earth simulations at historic CO₂ concentration (v-r, solid lines) and at present-day CO₂ concentration (vc-c, dotted lines). The α values represent the probability of exceedence, indicating that the temperature trends for the NH mid latitudes and tropics are both tested significantly different from 0 with the Student t-test

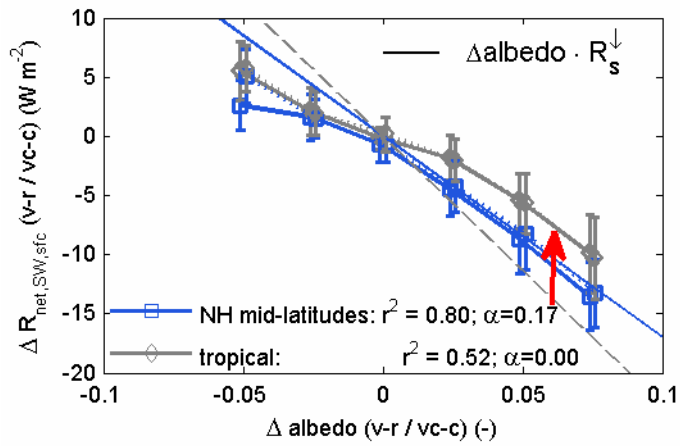


Fig 4 The change in net surface shortwave radiation as a function of change in albedo computed from the difference between the EC-Earth simulations at historic (v-r, solid lines) and at present-day CO₂ concentration, SST and SIC (vc-c, dotted lines). The thin lines without markers represent the direct shortwave radiative effect of albedo change: incoming SW radiation $\times (1 - \Delta\text{albedo})$, thus including the effect of clouds in the reference simulation (solid: NH mid-latitudes, dashed: tropics). The deviation from the straight line (red arrow) indicates the impact of feedbacks. The figure applies to the surface, but is very similar for the TOA. The actual changes in net radiation are significantly different from the expected ones, with exceedance probabilities α

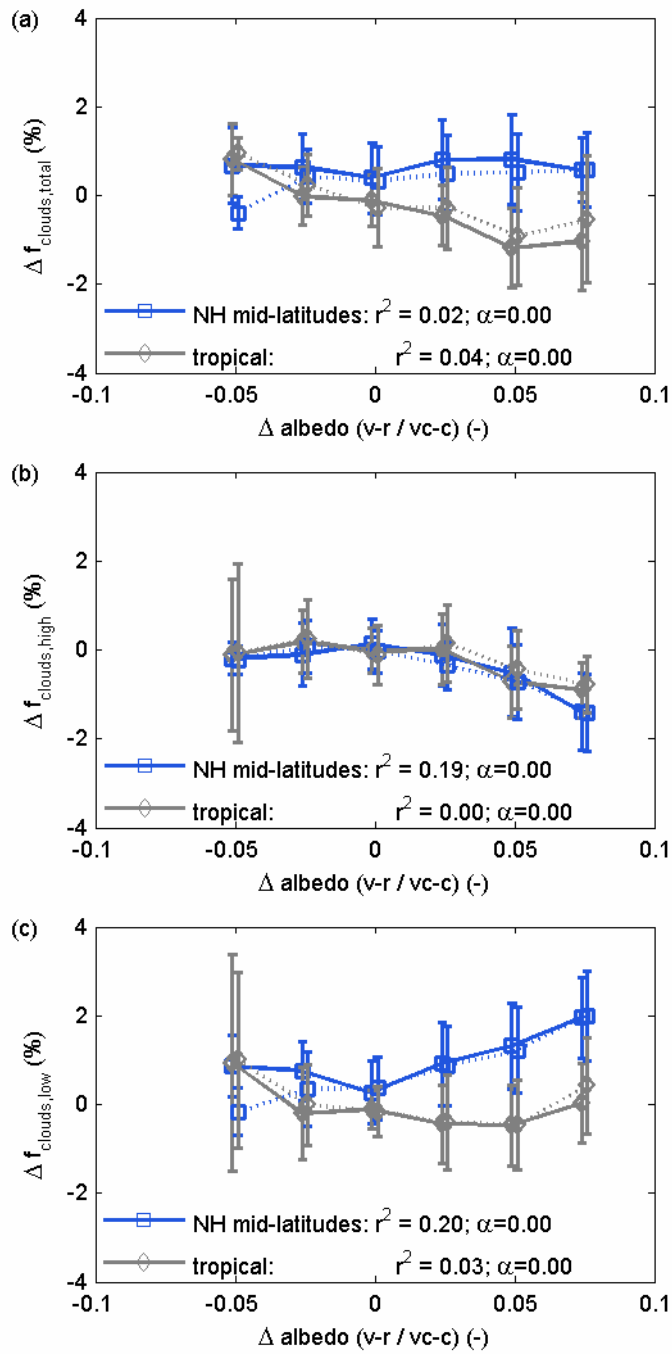


Fig 5 The change in **a** total, **b** high and **c** low cloud cover fraction as a function of change in albedo computed from the difference between the EC-Earth simulations at historic CO₂ concentration (v-r, solid lines) and at present-day CO₂ concentration (vc-c, dotted lines) . α indicates the exceedence probability of the slopes relative to a flat line

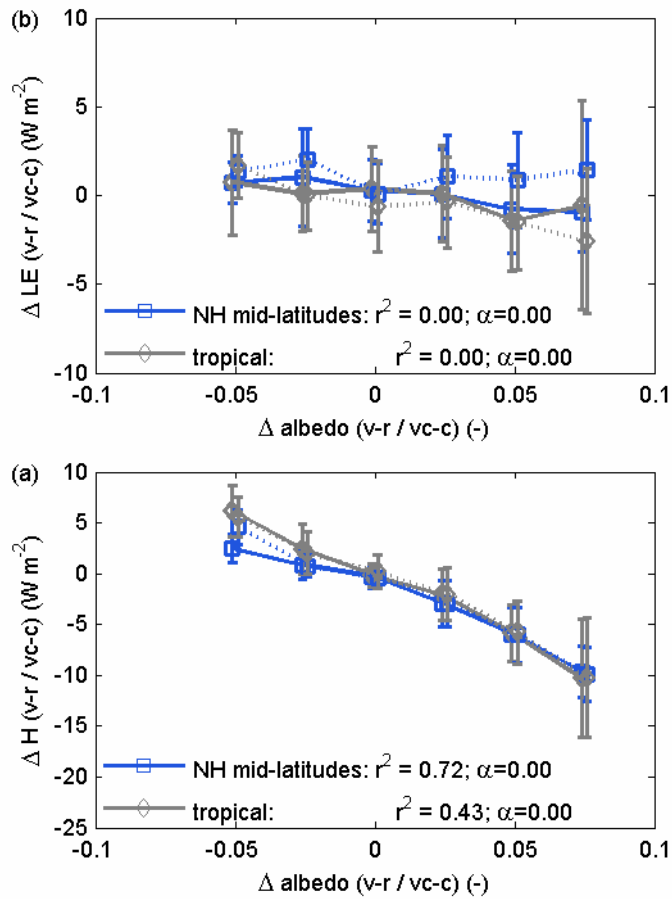


Fig 6 The change in surface sensible **a** and latent **b** heat flux as a function of the change in computed as the difference between the EC-Earth simulations at historic CO₂ concentration (v-r, solid lines) and at present-day CO₂ concentration (vc-c, dotted lines). α indicates the exceedence probability of the slope of the linear regression line on the raw data

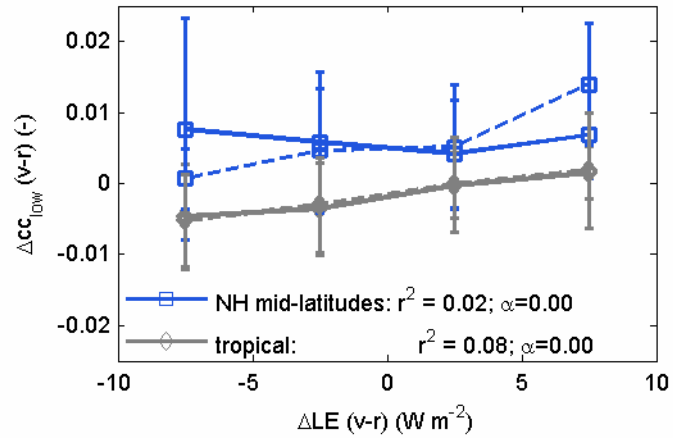


Fig 7 The change in low cloud fraction as a function of the change in latent heat flux between the EC-Earth simulations at historic CO₂ concentration (v-r, solid lines) and at present-day CO₂ concentration (vc-c, dotted lines). α indicates the exceedence probability of the slope of the linear regression line on the raw data

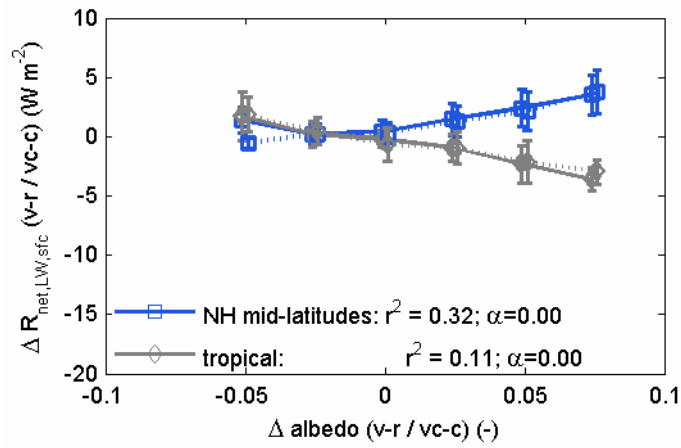


Fig 8 The change in net longwave radiation as a function of the change in albedo computed as the difference between the EC-Earth simulations at historic CO₂ concentration (v-r, solid lines) and at present-day CO₂ concentration (vc-c, dotted lines). α indicates the exceedence probability of the slope of the linear regression line on the raw data

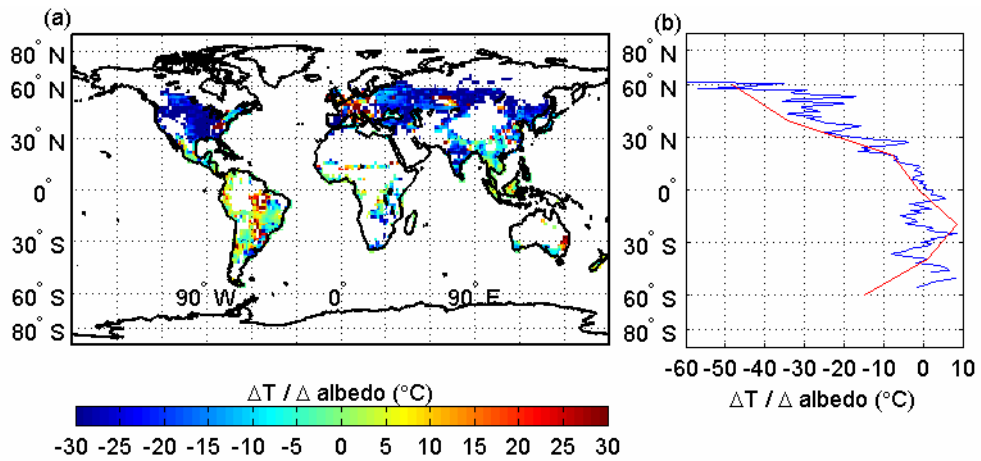


Fig 9 a spatial distribution of climate response to land cover change, scaled with the albedo change. Albedo change and temperature response are computed on a monthly basis and displayed as annual mean. Areas where the albedo change is less than 0.002 are masked out b zonal average climate response: the blue line represents the zonal average of the numbers displayed in (a), and the red line represents the zonal average $\Delta T / \Delta \text{albedo}$ over land, thus including non-local temperature changes, over latitudinal bands of 20° to reduce cross-zonal temperature advection